Electronic Supporting Information

Sharp Cu@Sn nanocones on Cu foam for highly selective and efficient electrochemical reduction of CO_2 to formate

Chengzhen Chen[a], Yuanjie Pang[b], Fanghua Zhang[a], Juhua Zhong[c], Bo Zhang*[d] and Zhenmin Cheng*[a]

a State Key Laboratory of Chemical Engineering, School of Chemical Engineering, East China University of Science and Technology, Shanghai 200237, China.

b School of Optical and Electronic Information, Huazhong University of Science and Technology, Wuhan, Hubei 430074, China.

c Department of Physics, East China University of Science and Technology, Shanghai 200237, China.

d State Key Laboratory of Molecular Engineering of Polymers, Department of Macromolecular Science, Fudan University, Shanghai 200438, China.

Corresponding Author

*E-mail: zmcheng@ecust.edu.cn& bozhang@fudan.edu.cn

Supplementary figures and tables

Table S1. The bulk pH of aqueous electrolytes after CO_2 saturation.

Electrolytes	Bulk pH after CO_2 saturation
0.1 M $KHCO_3$	6.83
0.05 M KCl+0.1 M $KHCO_3$	6.80
0.1 M KCl+0.1 M $KHCO_3$	6.79
0.2 M KCl+0.1 M $KHCO_3$	6.77
0.3 M KCl+0.1 M $KHCO_3$	6.76

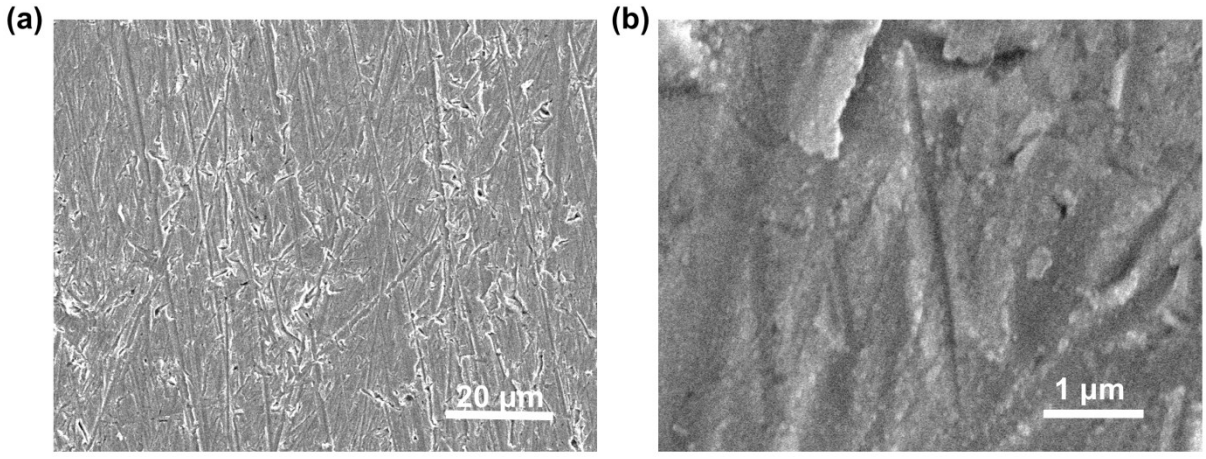

Fig. S1 (a) Low-magnification and (b) high-magnification SEM images of the Cu foil after pretreatment.

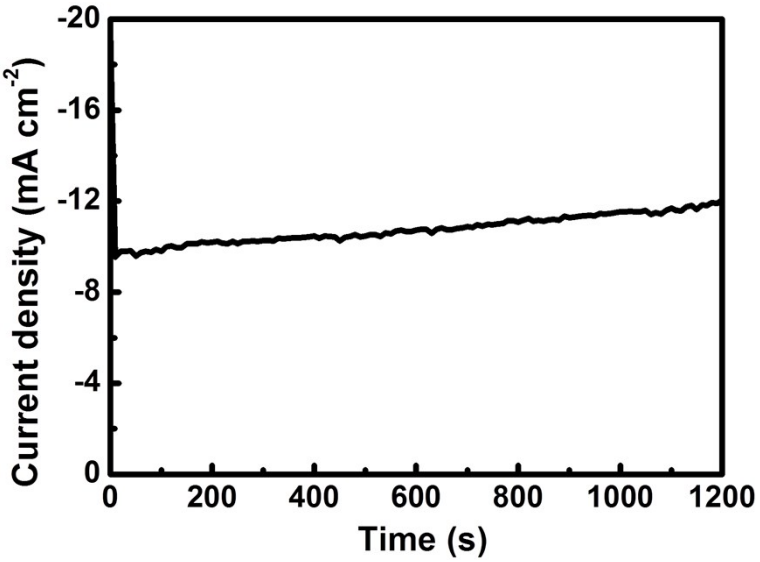

Fig. S2 Chronoamperometry curve for the electrodeposition of Cu-Ni nanocones precursor on Cu foil.

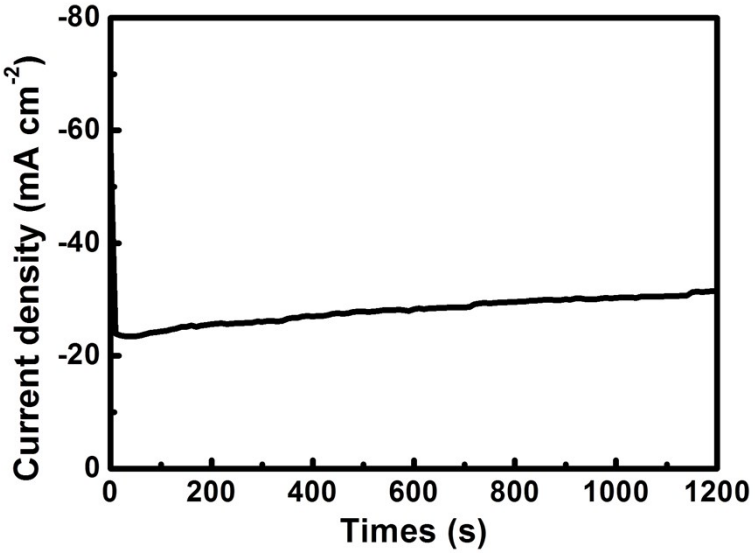

Fig. S3 Chronoamperometry curve for the electrodeposition of Cu-Ni nanocones precursor on Cu foam.

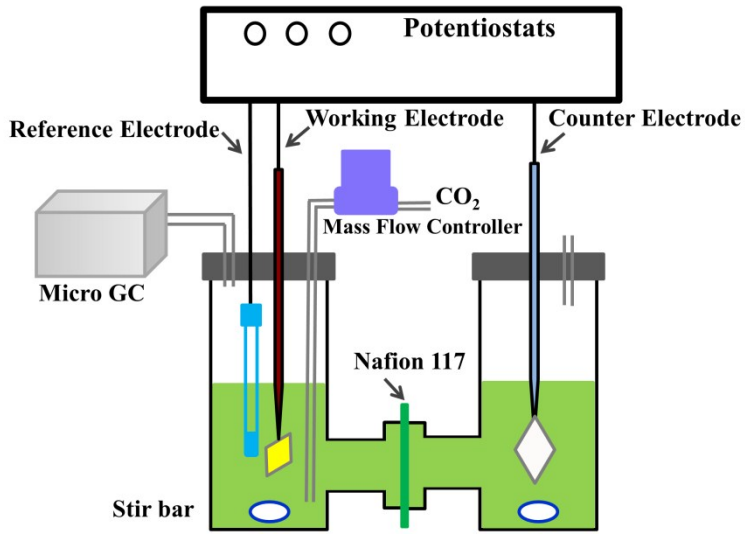

Fig. S4 Schematic illustration of a two-compartment electrolysis cell.

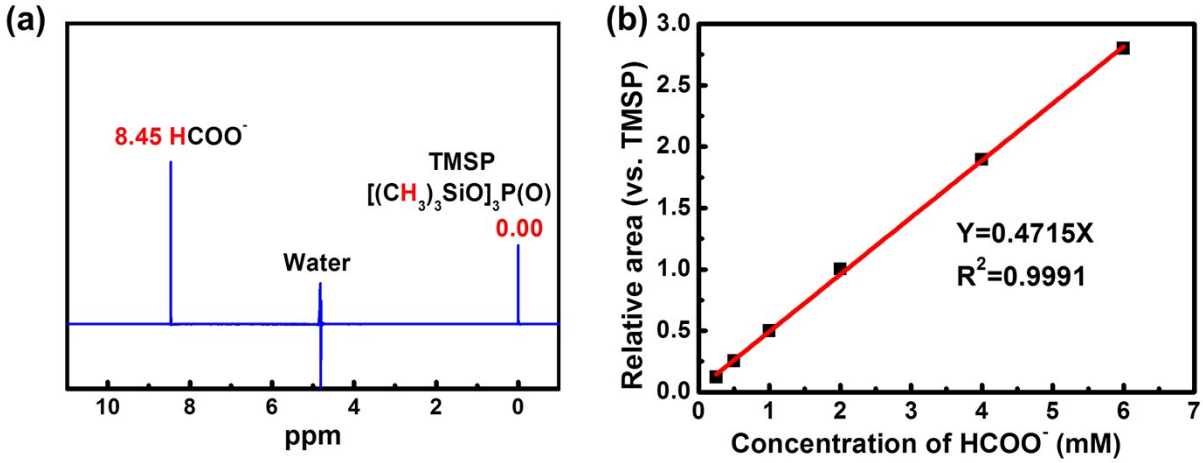

Fig. S5 (a) ^{1}H-NMR spectrum for a standard formate sample (4 mM); (b) the linear relationship between the standard formate concentration and relative area vs. TMSP. The relative areas were estimated by following equation:

$$\text{Relative area (formate)} = \frac{\text{peak area at 8.45 ppm (formate)}}{\text{peak area at 0.00 ppm (TMSP)}}$$

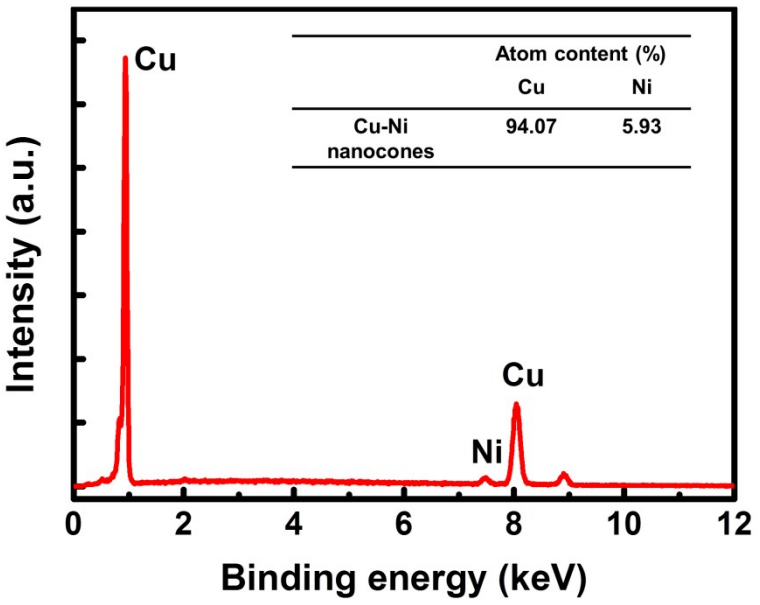

Fig. S6 Energy-dispersive X-ray spectra of Cu-Ni nanocones precursor on Cu foil.

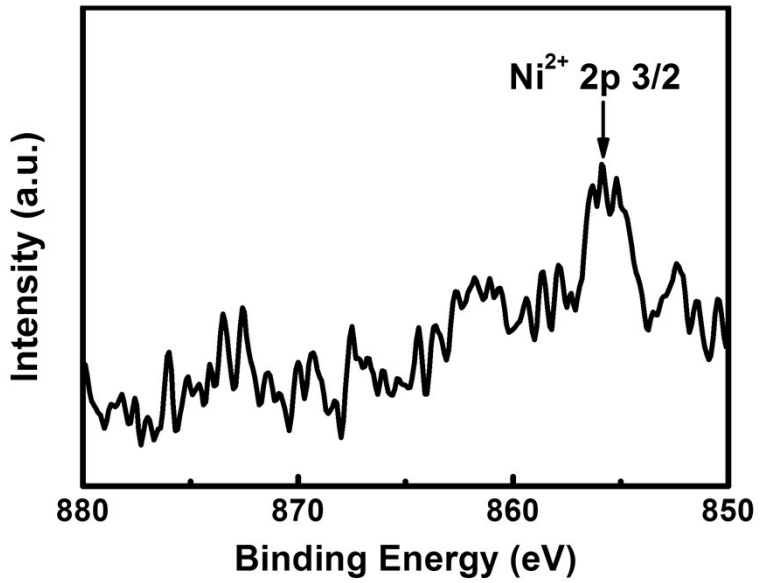

Fig. S7 High-resolution XPS spectra for the Ni 2p region of Cu-Ni nanocones.

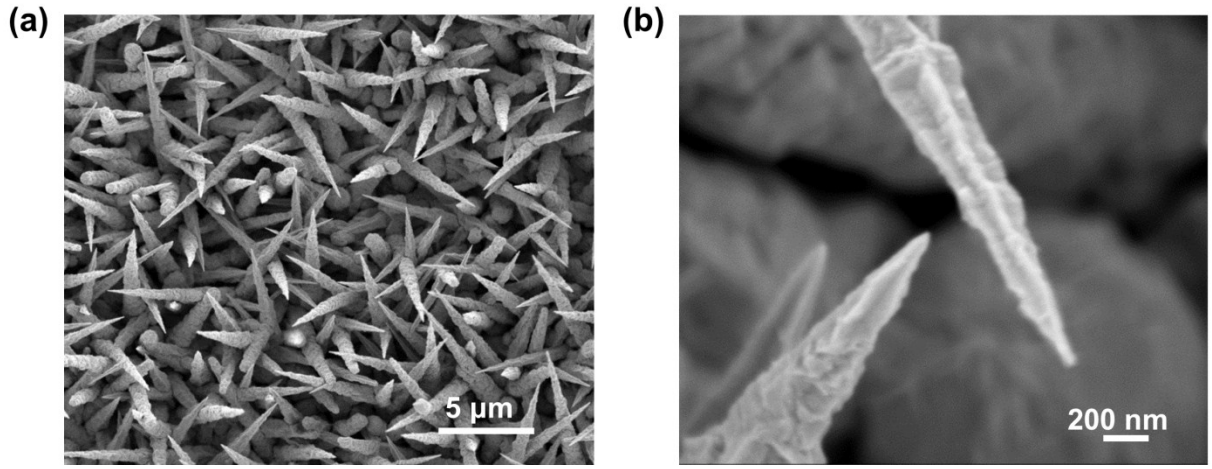

Fig. S8 (a) Low-resolution and (b) high-resolution SEM images of Cu-Ni nanocones precursor on Cu foil.

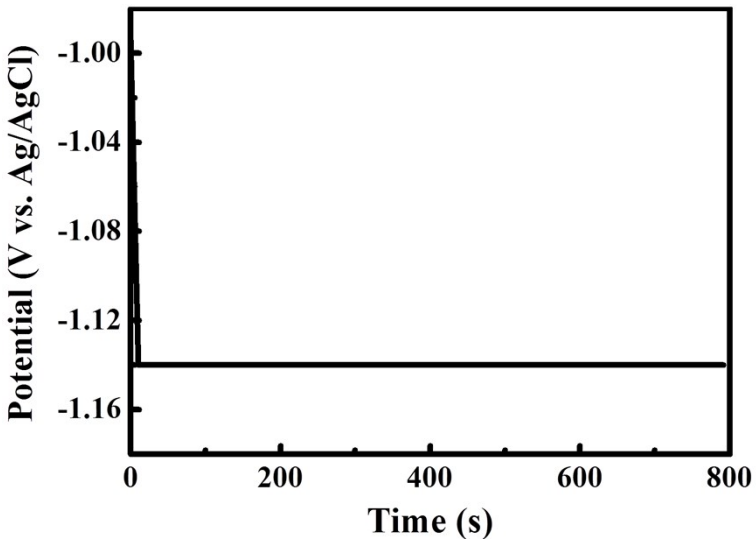

Fig. S9 Potential curve for the deposition of Sn on the Cu nanoconic surface at a constant current density of 3.3 mA cm^{-2} to prepare the Cu@Sn nanocones.

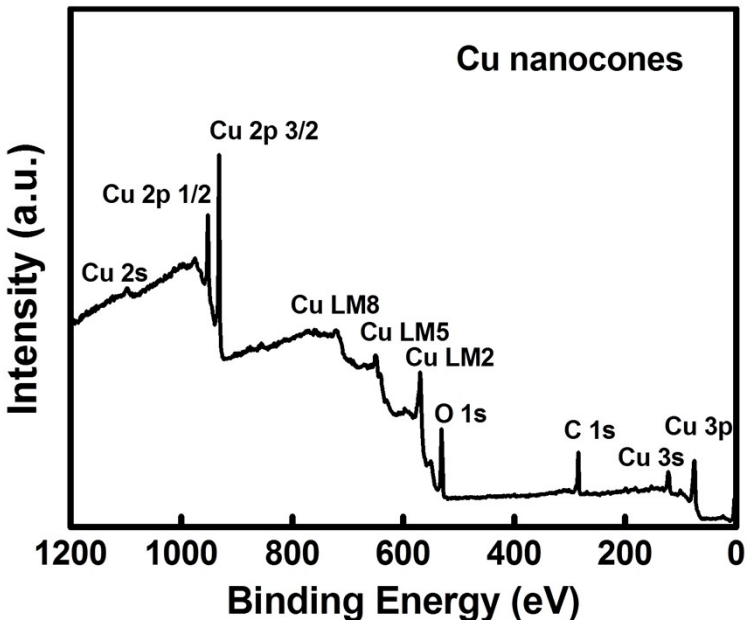

Fig. S10 XPS survey spectra of Cu nanocones.

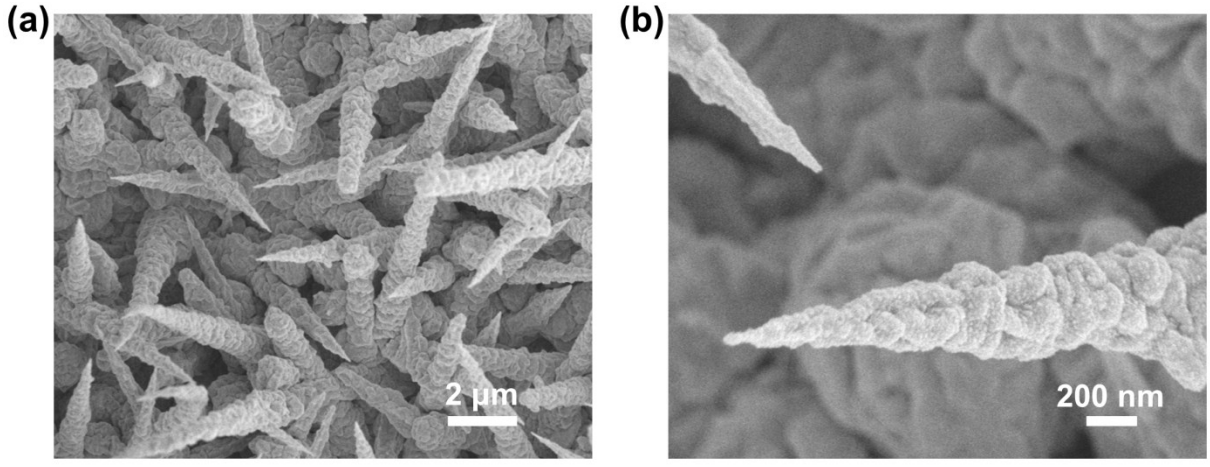

Fig. S11 (a) Low-resolution and (b) high-resolution SEM images of Cu nanocones precursor.

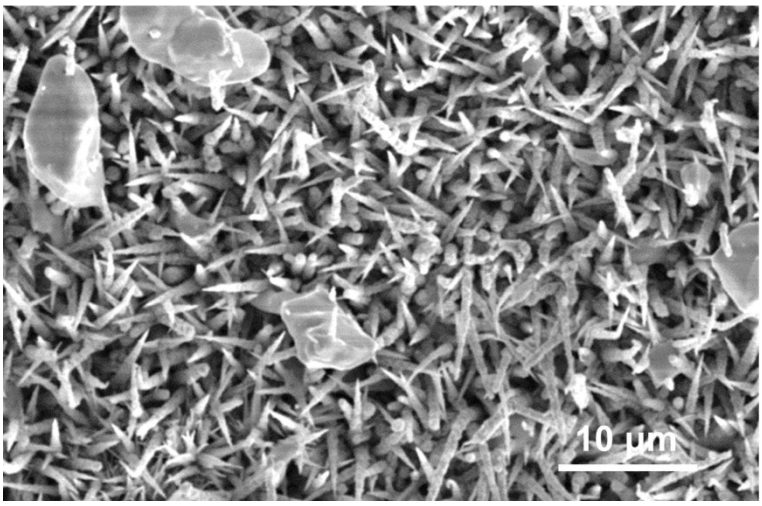

Fig. S12 SEM image of a small amount of bulk Sn lying above the Cu@Sn nanocones layer.

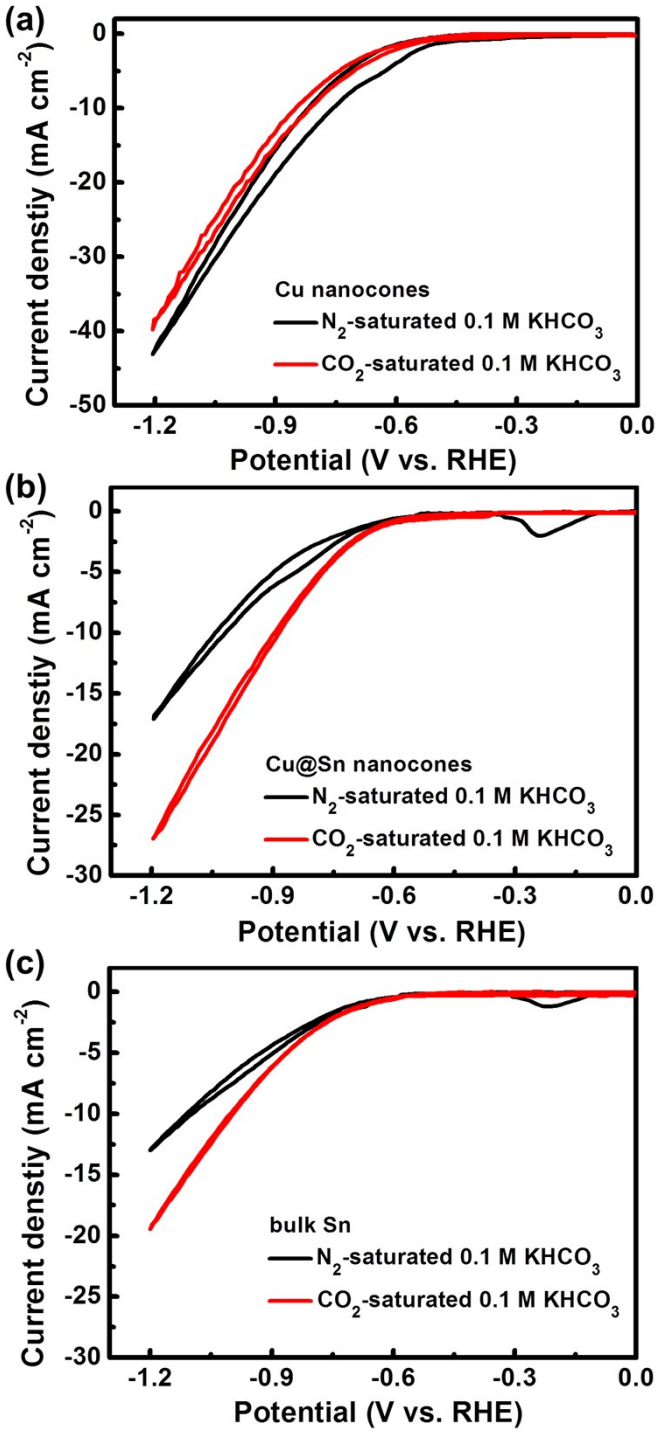

Fig. S13 Cyclic voltammogram curves (scan rate: 20 mV s^{-1}) in N_2 or CO_2 saturated 0.1 M $KHCO_3$ electrolyte of (a) Cu nanocones, (b) Cu@Sn nanocones with Sn deposition time of 800 s, (c) bulk Sn.

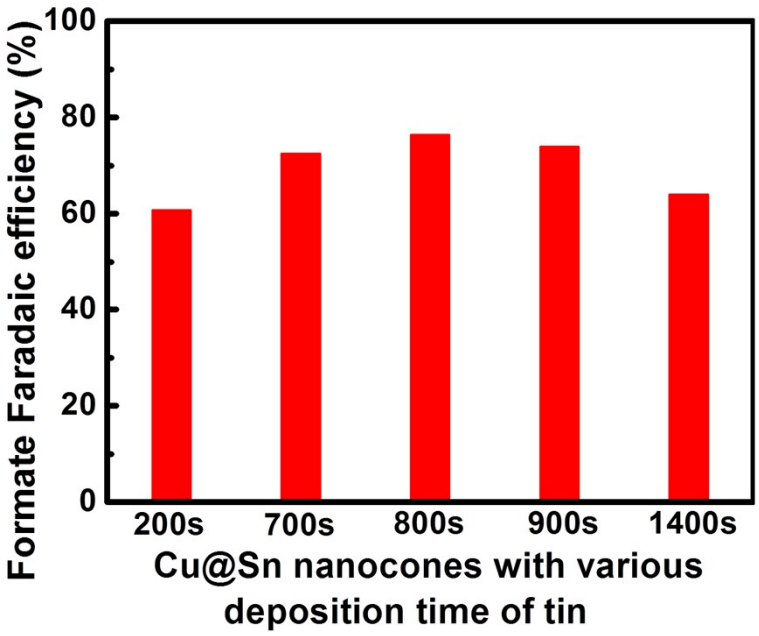

Fig. S14 Effect of Sn deposition time on formate faradaic efficiency with Cu@Sn nanocones at -0.9 V.

To optimize the electrocatalytic performance, Cu@Sn nanocones electrodes differing in the Sn deposition time were prepared and subsequently tested at -0.9 V in CO_2-saturated 0.1 M $KHCO_3$. The gaseous product and liquid product were determined using gas chromatography (GC) and NMR spectrometer, respectively. Interestingly, the formate faradaic efficiency rose significantly with prolonging the Sn deposition time, reaching a maximum value of 67.6% at deposition time of 800s (Fig. S14), and then decreased with further elongating the time to 1400s, accompanied with the increased density of bulk Sn above the nanocones layer (Fig. S15). Thus, the Cu@Sn nanocones with tin deposition of 800s was used for all physical characterization and labelled as Cu@Sn nanocones on the whole work.

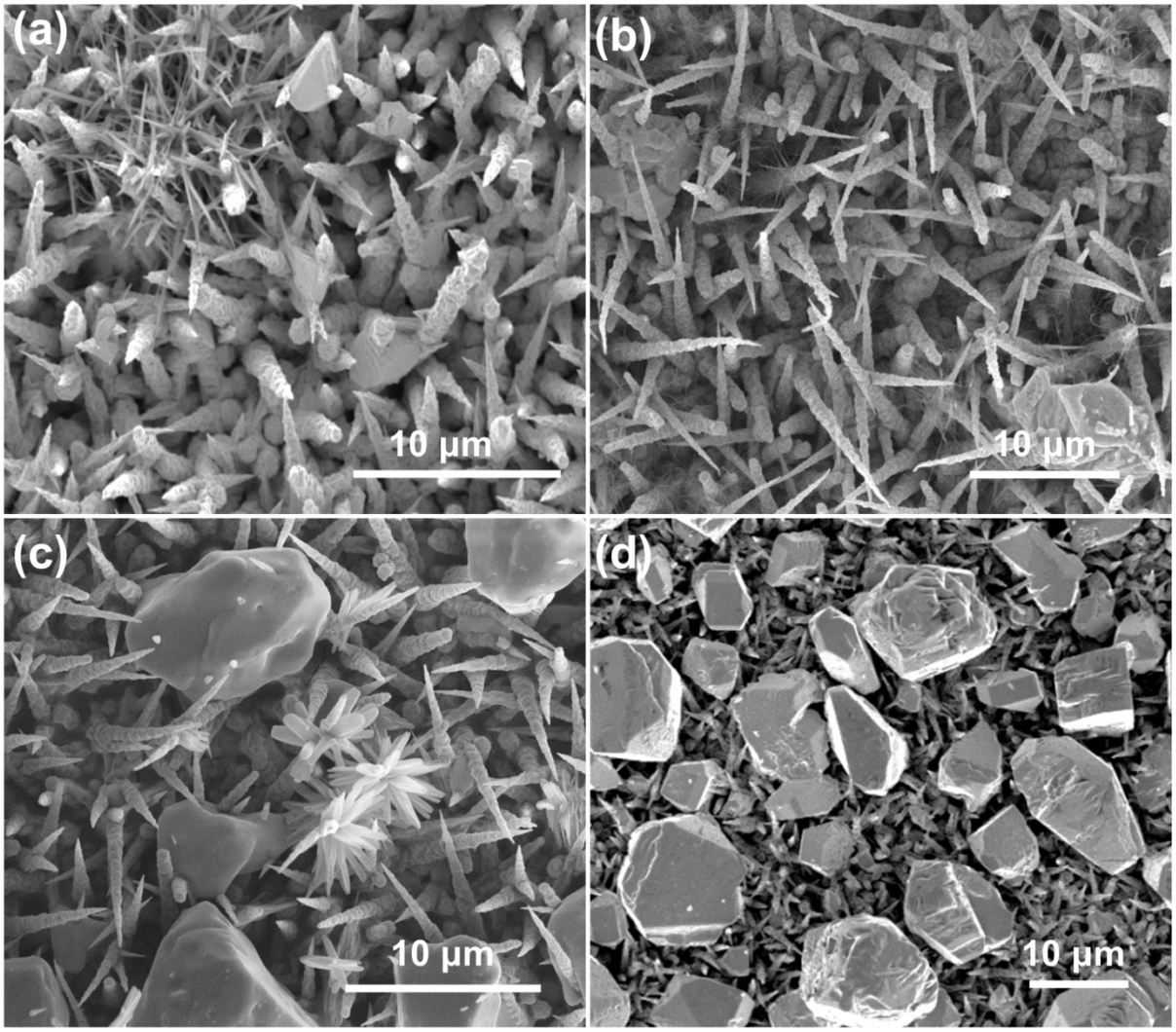

Fig. S15 SEM images of Cu@Sn nanocones with various Sn deposition time of (a) 200 s, (b) 700 s, (c) 900 s, (d) 1400 s.

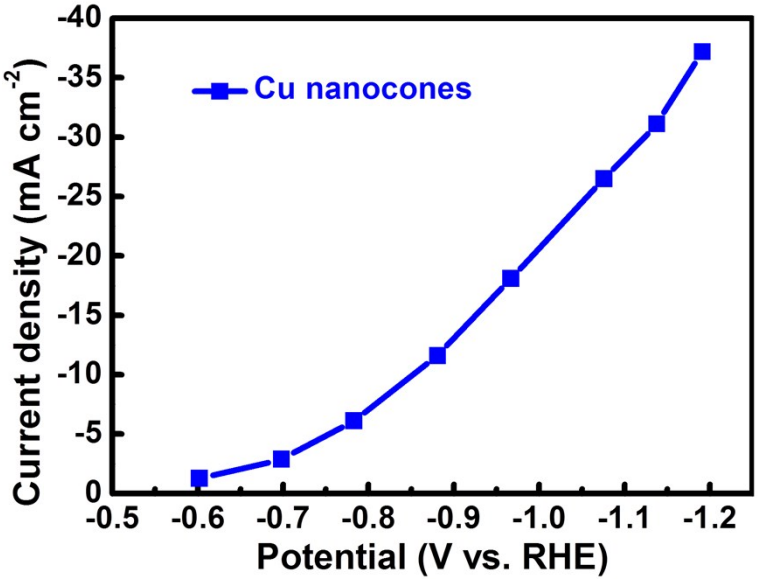

Fig. S16 Total current density of Cu nanocones at various potentials measured in CO_2-saturated 0.1 M $KHCO_3$.

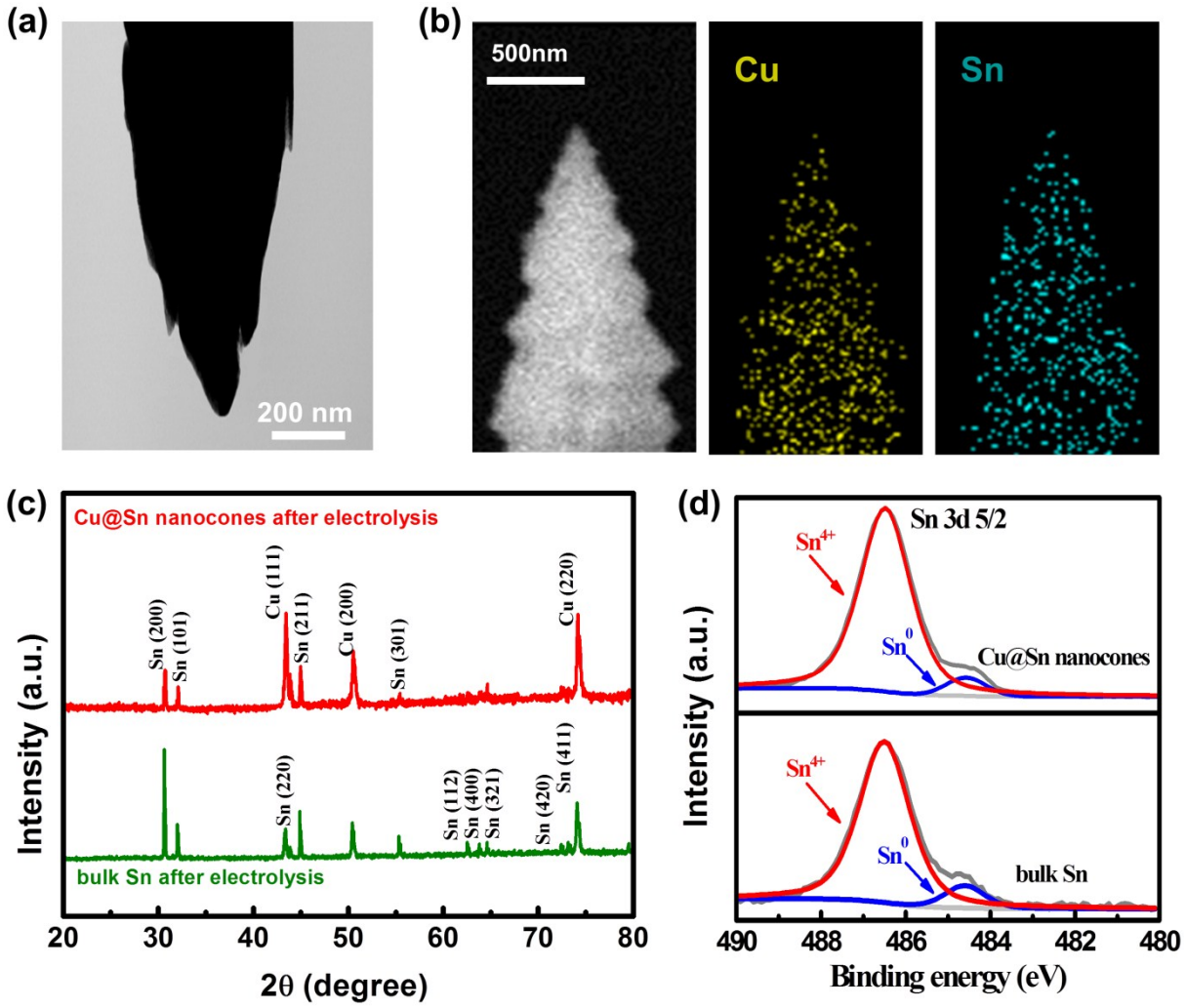

Fig. S17 (a) TEM image, (b) SEM-EDS mapping of Cu@Sn nanocone after electrolysis; (c) XRD patterns, (d) Sn 3d 5/2 XPS spectra of Cu@Sn nanocones and Sn particles after electrolysis.

After CO_2 electrolysis, the conical structure of Cu@Sn nanocones was retained, with deposited Sn well preserved (Fig. S17a and S17b). Meanwhile, no other peaks were observed in the XRD data except for the peaks of bulk metallic copper and tin ((JCPDS 86-2265)) (Fig. S17c), while the exposure of surface Sn to air before XPS measurements led to the spontaneous and partial oxidation (Fig. S17d).

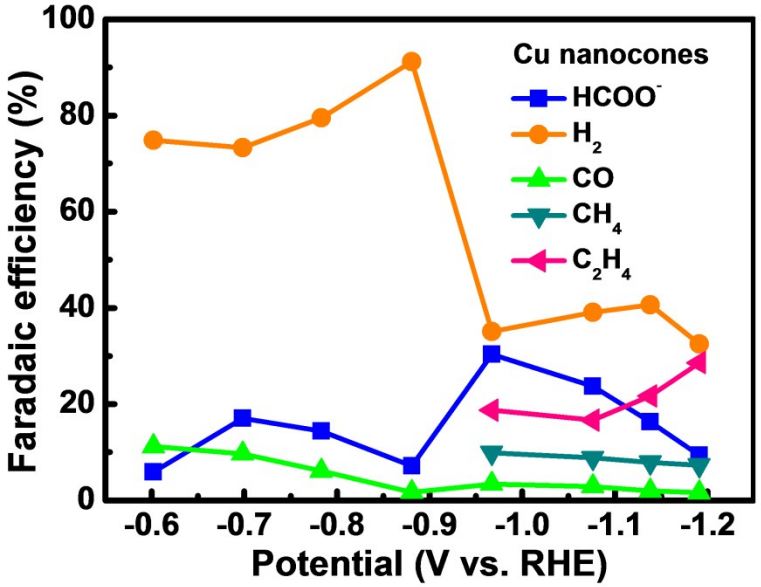

Fig. S18 Faradaic efficiency of different products on Cu nanocones at various applied potentials.

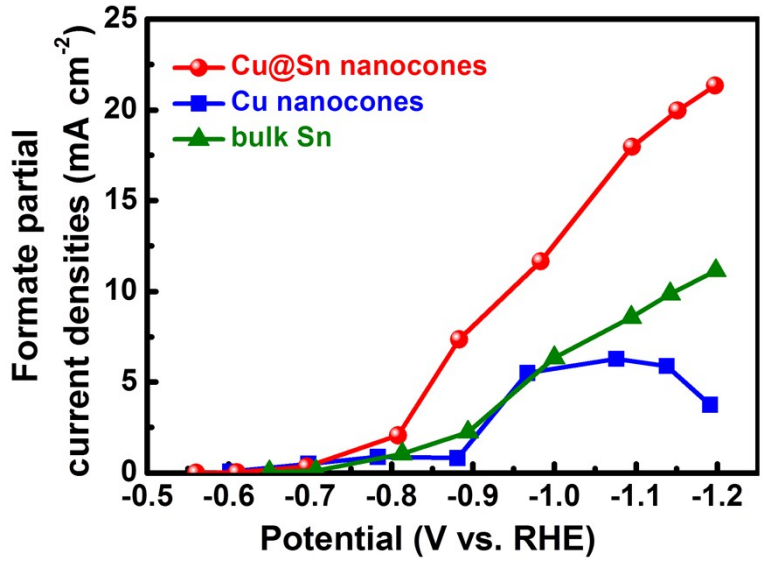

Fig. S19 Formate partial current density of Cu@Sn nanocones and bulk Sn at various potentials.

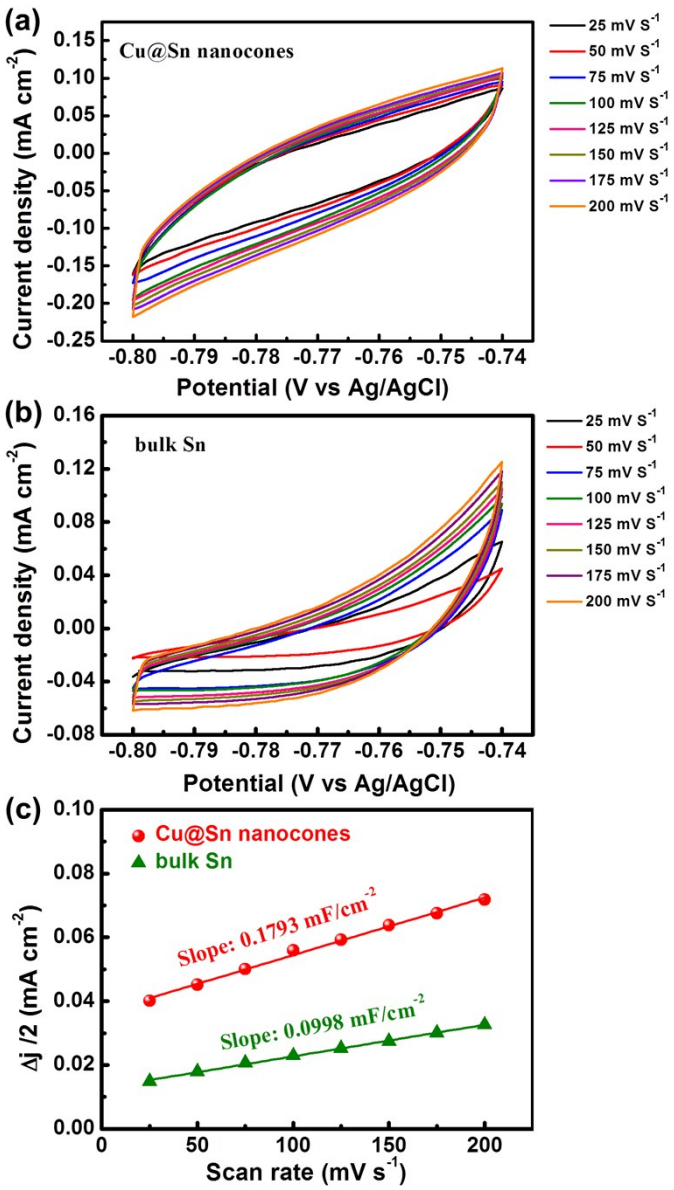

Fig. S20 (a) Cu@Sn nanocones, (b) Sn particles charging current density plotted against various CV scan rates; (c) double layer capacitance plots. The electrochemical surface area (ECSA) was estimated from the double-layer capacitance (C_{dl}) of different catalysts in N_2-satarated 0.1 M $KHCO_3$. Cyclic voltammetry was record in a potential window where only double layer charging and discharging happened. Plotting the $\triangle j/2$ ($(j_a-j_c)/2$) at the middle point of potential window against CV scan rates would acquire the C_{dl}, where j_a and j_c are the corresponding anodic and cathodic current density.

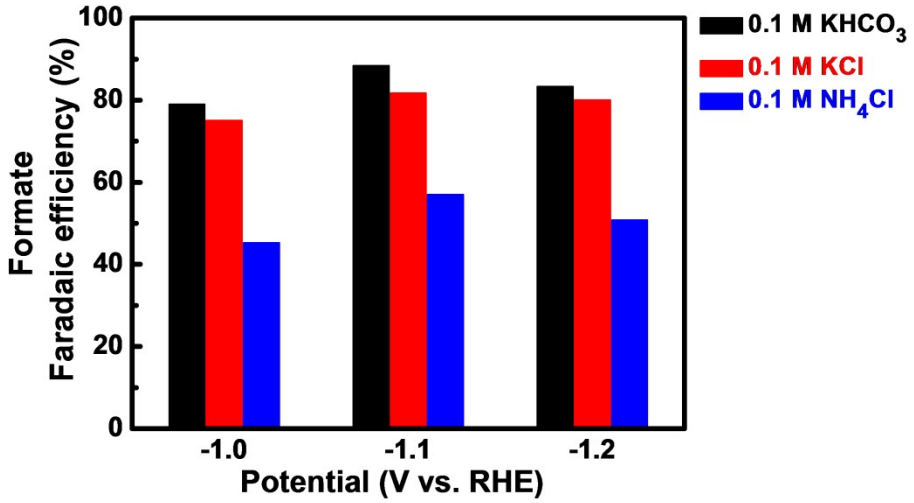

Fig. S21 Formate faradaic efficiency of Cu@Sn nanocones in different electrolytes.

The CO_2 reduction on Cu@Sn nanocones in 0.1 M KCl electrolyte were also performed (Fig. S21). It shows that formate faradaic efficiency (FE) was slightly decreased in the KCl electrolyte compared to that in $KHCO_3$ solution. A similar phenomenon also has been observed in nanostructured Ag catalyst.[1]

To get a better focus on Cl^- and eliminate the beneficial effect of K^+, CO_2 experiments on Cu@Sn nanocones were carried out in 0.1 M NH_4Cl electrolyte. The results show that formate FE was dramatically declined only with the presence of Cl^- (Fig. S21).

These results together confirm that the increament of K^+ concentration was responsible for the improved formate selectivity in Fig. 4e

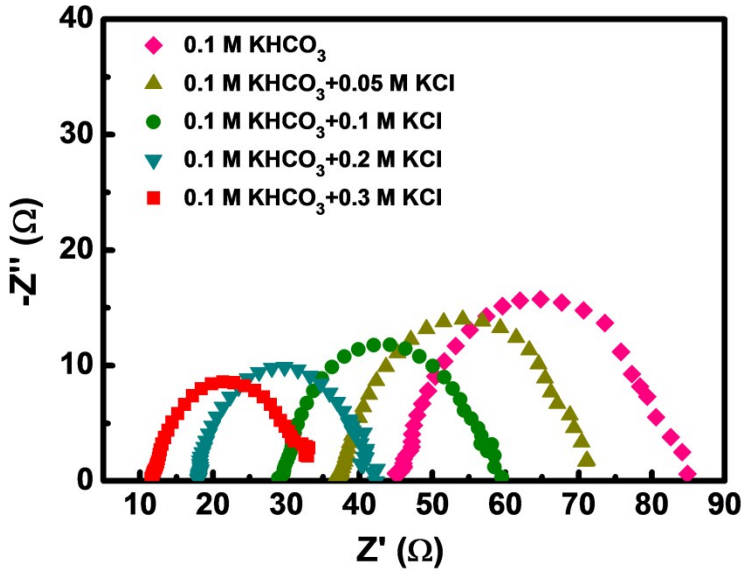

Fig. S22 Nyquist plots of Cu@Sn nanocones in CO_2-saturated electrolyets in a frequency range from 1 MHz to 0.05 Hz with 10 mV amplitude at -0.95 V vs. RHE

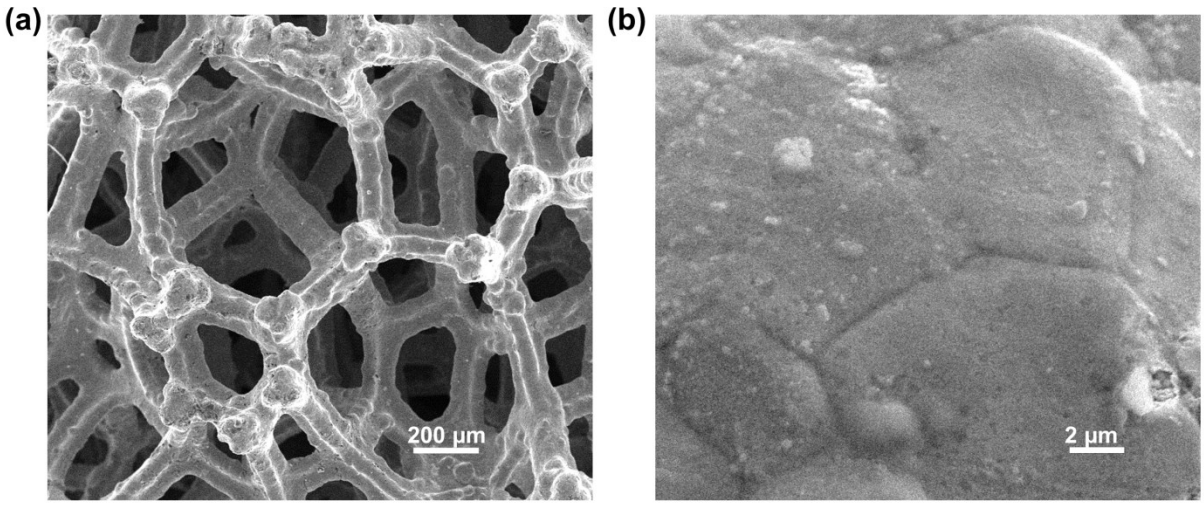

Fig. S23 (a) Low-magnification and (b) high-magnification SEM images of Cu foam substrate.

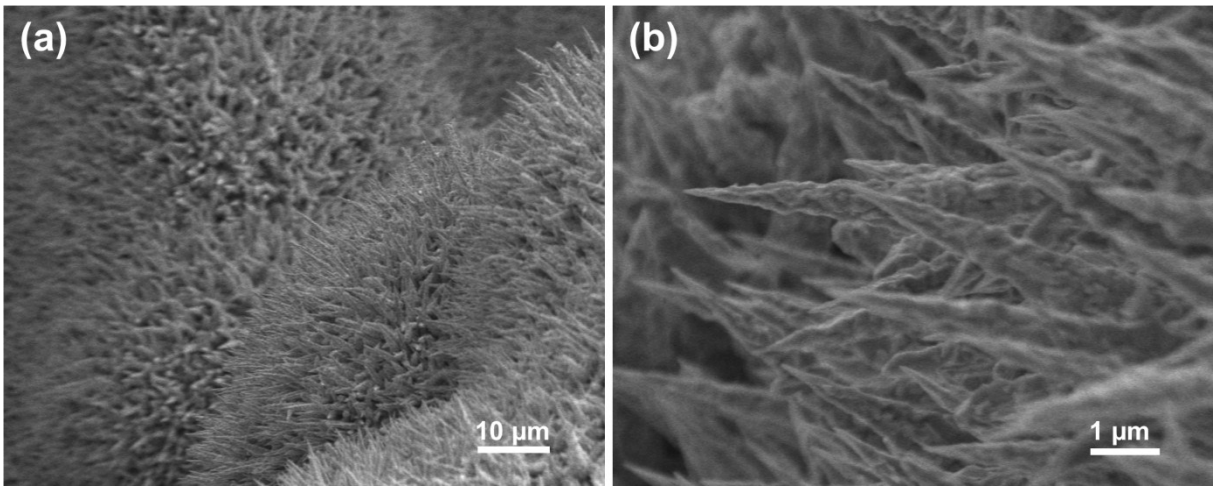

Fig. S24 (a) Low-magnification and (b) high-magnification SEM images of Cu-Ni nanocones precursor over Cu foam.

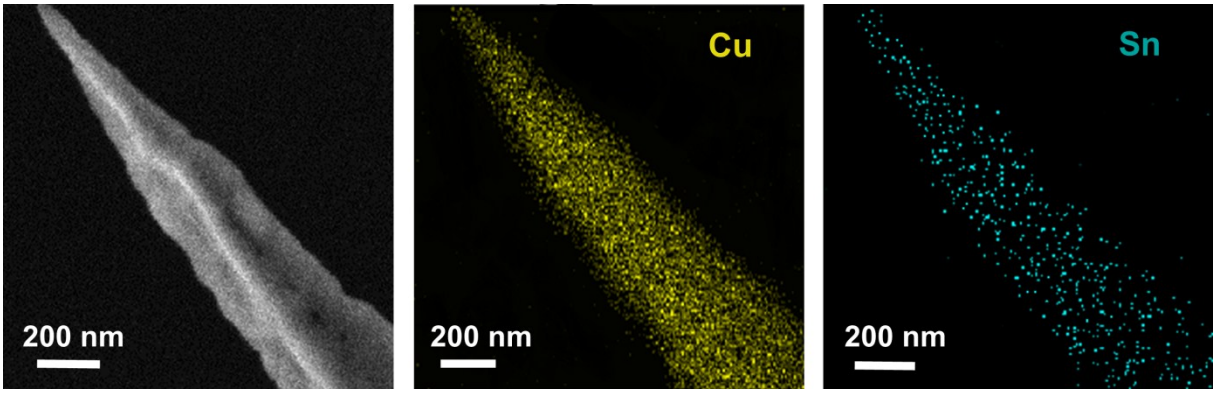

Fig. S25 SEM-EDS mapping results of Cu@Sn nanocones/Cu foam catalysts.

According to the ratio of average current density in depositing Cu-Ni nanocones on Cu foam relative to Cu foil (Fig. S2 and Fig. S3), the deposition time of Sn was prolonged to 2100 s for Cu@Sn nanocones/Cu foam electrode.

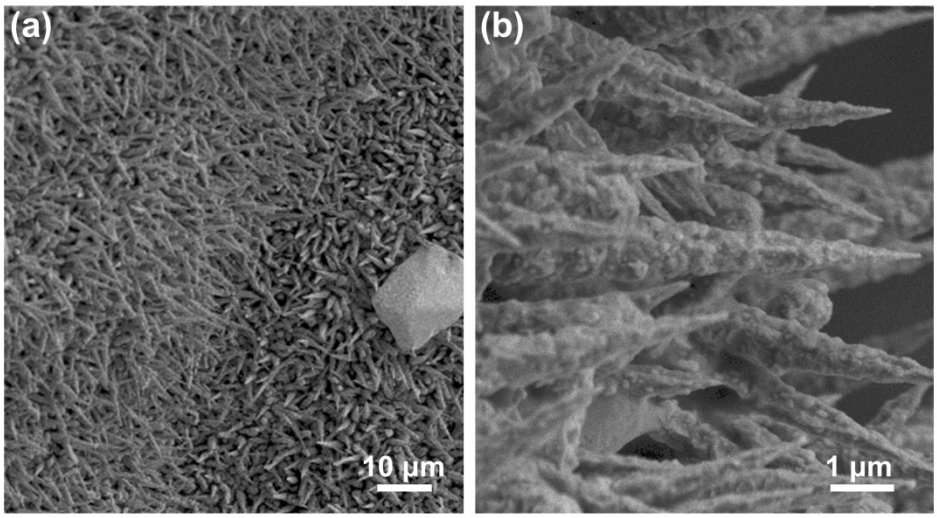

Fig. S26 (a) Low-magnification and (b) high-magnification SEM images of Cu@Sn nanocones catalyst after 10 h reaction.

Table S2. Comparison of the electrocatalytic performance of noble-metal-free Sn-based catalysts.

Catalysts	Electrolytes	Potential[a] (V vs. RHE)	Faradaic efficiency (%)[b]	Current density (mA cm^{-2})[c]	Tafel slope (mV dec^{-1})	Reference
Cu@Sn nanocones/Cu foam	0.1 M $KHCO_3$ +0.3M KCl	-1.10	90.4	57.7	Not studied	This work
Cu@Sn nanocones/Cu foil	0.1 M $KHCO_3$	-1.10	88.4	20.4	80.1	This work
SnO_2 nanosheets/carbon cloth	0.5 M $KHCO_3$	-0.95	89	48.6	79	Li et al.[2]
Sn particle/carbon nanotube areogel	0.5 M $KHCO_3$	-0.96	82.7	26.7	155	Chen at al.[3]
Nanoporous tin foam	0.1 M $NaHCO_3$	-1.30	90	23.5	Not studied	Du et al.[4]
Metallic tin quantum sheets	0.1 M $NaHCO_3$	-1.15	89	21.1	83	Lei et al.[5]
Tin dendrite	0.1 M $KHCO_3$	-1.36	71.6	17.1	145	Won et al.[6]
SnS_2 nanosheets	0.5 M $NaHCO_3$	-0.8	84.5	13.9	83	Li et al.[7]
SnO_2 nanoparticles	0.1 M $NaHCO_3$	-1.15	93.6	10.2	70	Zhang et al.[8]
SnO_2 porous nanowires	0.1 M $NaHCO_3$	-1.0	76	10	134	Kumar et al.[9]
Porous tin film	0.1 M $KHCO_3$	-1.2	91.5	5.5	Not studied	Lu et al.[10]
Thin SnO_x/Sn layer	0.1 M $KHCO_3$	-1.09	77.4	4.8	146	Daiyan et al.[11]
Deposited Sn particles	0.1 M $KHCO_3$	-1.15	63	4.5	169	Zhao et al.[12]
Sn foil	0.5 M $NaHCO_3$	-0.7	0.3	3	74	Chen et al.[13]

[a] Applied potential at the maximum faradaic efficiency. [b] Maximum faradaic efficiency.

[c] Total current density at the maximum faradaic efficiency.

REFERENCES

1.S. Verma, X. Lu, S. Ma, R. I. Masel and P. J. Kenis, *Phys. Chem. Chem. Phys*., 2016, **18**, 7075-7084.

2. F. Li, L. Chen, G. P. Knowles, D. R. MacFarlane and J. Zhang, *Angew. Chem. Int. Ed.*, 2017, **56**, 505-509.

3. Z. Chen, S. Yao and L. Liu, *J. Mater. Chem. A*, 2017, **5**, 24651-24656.

4. D. Du, R. Lan, J. Humphreys, S. Sengodan, K. Xie, H. Wang and S. Tao, *Chemistryselect*, 2016, **1**, 1711-1715.

5. F. Lei, W. Liu, Y. Sun, J. Xu, K. Liu, L. Liang, T. Yao, B. Pan, S. Wei and Y. Xie, *Nat. Commun.*, 2016, **7**, 12697.

6. H. Won da, C. H. Choi, J. Chung, M. W. Chung, E. H. Kim and S. I. Woo, *ChemSusChem*, 2015, **8**, 3092-3098.

7. F. Li, L. Chen, M. Xue, T. Williams, Y. Zhang, D. R. MacFarlane and J. Zhang, *Nano Energy*, 2017, **31**, 270-277.

8. S. Zhang, P. Kang and T. J. Meyer, *J. Am. Chem. Soc.*, 2014, **136**, 1734-1737.

9. B. Kumar, V. Atla, J. P. Brian, S. Kumari, T. Q. Nguyen, M. Sunkara and J. M. Spurgeon, *Angew. Chem. Int. Ed.* , 2017, **56**, 3645-3649.

10.W. Lv, J. Zhou, F. Kong, H. Fang and W. Wang, *INT J HYDROGEN ENERG*, 2016, **41**, 1585-1591.

11. R. Daiyan, X. Lu, Y. H. Ng and R. Amal, *Catal. Sci. Technol.*, 2017, **7**, 2542-2550.

12. C. Zhao and J. Wang, *Chem. Eng. J.*, 2016, **293**, 161-170.

13. Y. Chen and M. W. Kanan, *J. Am. Chem. Soc.*, 2012, **134**, 1986-1989.